Microgrids Physics Model-based Fault Location Formulation: Analytic-based Distributed Energy Resources Effect Compensation

A. S. Bretas, C. Orozco-Henao, J. Marín-Quintero, O. Montoya, W. Gil, N. G. Bretas

***Abstract*— Distributed energy resources consideration by fault location formulations is a technical challenge. Stochastic behavior complicates deterministic solutions, while probabilistic approaches are yet to be fully explored. This paper presents analytical physics-based models towards the solution to this challenge. Presented models consider information availability from distributed energy resources to improve the fault location reliability. Information considered is divided into two categories: synchronized measurements provided by intelligent electronic devices located in the substation and in each terminal of distributed energy resources; and linear analytical-based models of distributed energy resources. Distributed energy resources models are used only when remote measurements are not available. Different distributed energy resources technologies and their operation modes are modeled. The presented fault location solution is validated on the *IEEE* 34-nodes test feeder modified. Easy-to-implement model, without hard-to-design parameters, built on the classical impedance-based fault location solution, indicates potential for real-life applications.**

Keywords— *Fault location; Microgrids; Distributed Energy Resources*.

I. Introduction

ACTIVE Distribution Networks (ADN) and Microgrids (MG) increase system resilience [1]. Their integration enables self-healing functionalities in which, the Fault Location (FL) plays an essential role [2]. In recent years, efforts have been dedicated towards the development of FL solutions for service restoration support and reduced outage time [3]. Regarding FL in distribution networks, four solutions have been highlighted in the literature: traveling waves-based methods [4], learning-based methods [5], [6], impedance-based methods [7]–[14] and hybrid-based methods [15].

Impedance-based methods [3] are easy-to-implement in real-life applications, mainly due to low cost requirements [7], [10], [14]. These techniques present some limitations, as the multiple estimation of the fault location, which can be addressed by hybrid methods [15].

With the deployment of ADN and MGs, inclusion of DER effects in the FL formulation has become inevitable. Most of these technologies require a power electronic based interface, referred in this paper as inverter-interfaced DER (IIDER), for grid connection. Other DER technologies can be connected directly to the grid, and they are referred in this work as Inverter non-interfaced DER (INIDER).

FL solutions which consider DER effects were initially presented in [15]–[24]. Considering [21], [22], one common aspect of these works is that the DER effect is considered by a synchronous machine model. However, this model is only valid for some types of DER, as INIDER.

Considering [15], [20], [23], FL is formulated considering wide-area synchronized current and voltage phasors measurements provided by digital fault recorders and Global Positioning System (GPS). These methods are robust, however depend strongly on the availability of the measurements at the DER location. Otherwise, [18], [24] use wide-area non-synchronized measurements, though they are still wide-area measurement dependent. On the other hand, in previous work of the authors [16], [17], [19], [23], models that uses both synchronized measurements and an IIDER model are presented. Although, these FL models only considers IIDER when working in limiting current operation mode.

Considering the aforementioned, this work presents analytical physics-based models towards the solution of the FL problem for MG. Simultaneously connected different DER technology types are considered. Wide-area measurements provided by Intelligent Electronic Devices (IEDs) located at the substation and the DER location are used. Likewise, linear analytical equivalent models are used to consider the DER effect in conditions when the information provided by IEDs are not available. A forward-backward sweep process is developed to estimate the DER current contribution to the fault location. The contributions of this work towards the state-of-the-art are:

- Analytical physics-based models for DER effect compensation on impedance-based fault location solutions;
- Consideration in the impedance-based FL formulation, of multiple simultaneous DER technologies types connected to the MG;

This work was supported in part by Ministry of Science, Technology and Innovation Announcement 757 of 2017 and announcement 852 - project Integra2023, code 111085271060, contract 80740-774-2020; and NSF ECCS # 1809738.

A. S. Bretas is with Department of Electrical and Computer Engineering, University of Florida, Gainesville, FL, USA; (arturo@ece.ufl.edu).
C. Orozco-Henao and J. Marín-Quintero are with Electrical and Electronic Engineering Department, Universidad del Norte, Barranquilla Colombia (chenaoa@uninorte.edu.co; jgmarin@uninorte.edu.co)
W. Gil is with Facultad de Ingeniería, Institución Universitaria Pascual Bravo, Medellín, Colombia (walter.gil@pascualbravo.edu.co)
O. Montoya is with Facultad de Ingeniería, Universidad Distrital Francisco José de Caldas, Bogotá D.C, Colombia (o.d.montoyagiraldo@ieee.org).
N. G. Bretas is with the Electrical and Computer Engineering, University of Sao Paulo, Brazil (ngbretas@sc.usp.br)
Paper submitted to the International Conference on Power Systems Transients (IPST2021) in Belo Horizonte, Brazil June 6-10, 2021.

- Adaptive solution considering or not wide-area measurements from distributed energy resources to improve the fault location.

The remainder of this paper is organized as follows. Section II presents the DER modelling. Section III presents the proposed generalized FL equations. Section IV presents the FL model and algorithm. Section V presents a case study. Section VI presents the results and discussion. Finally, Section VII presents the main conclusions of this work.

II. DER Modelling

The effect of DER technologies in impedance-based FL formulations can be modeled from their during-the-fault period behavior. Section A and B presents analytical models for each DER technology, while section C, extended models considering measurements provided by IEDs are introduced.

A. Inverter-interfaced DER (IIDER)

IIDER, such as electrochemical, storage and renewable devices use a power electronic interface to connect with MG. This interface has an inverter as its main device. In this work, the grid-connected inverter equivalent model [25] is used. This model is formulated for a two-level Voltage Source Inverter (VSI), which presents two operation modes: power set point track mode and limiting current mode. Equation (1) defines the current behavior of the IIDER, where if $I_{L_w} < I_{thld}$ the IIDER operates in power set point track mode, and if $I_{L,sat_w} \geq I_{thld}$ it operates in limiting current mode [25].

$$I_{s_w} = \begin{cases} \left(\frac{S_{ref}}{3 \cdot V_{s_w}^{(+)}}\right)^* - V_{s_w}^{(-)} \cdot j\omega C_f \; if \; I_{L_w} < I_{thld} \\ I_{L,sat_w} - V_{s_w} \cdot j\omega C_f \; if \; I_{L,sat_w} \geq I_{thld} \end{cases} \quad (1)$$

With,

$$I_{L_w} = \left(\frac{S_{ref}}{3 \cdot V_{s_w}^{(+)}}\right)^* + V_{s_w}^{(+)} \cdot j\omega C_f \quad (2)$$

$$I_{L,sat_w} = 2 \cdot I_{DERrate} \quad (3)$$

where, superscripts (+) and (-) represent the positive and negative sequence component of the electrical properties respectively, $*$ denotes a complex conjugate, V_{s_w} is the grid voltage for the phase w, C_f is the filter capacitor, ω is the angular frequency , I_{L_w} the inductor current references, $I_{DERrate}$ the inverter nominal current, I_{L,sat_w} saturation current of the inverter, I_{thld} the inductor current threshold, and I_{s_w} is output current of IIDER.

B. Inverter non-interfaced DER (INIDER)

INIDER can be modeled through a synchronous generator model, as illustrated in Fig. 1.

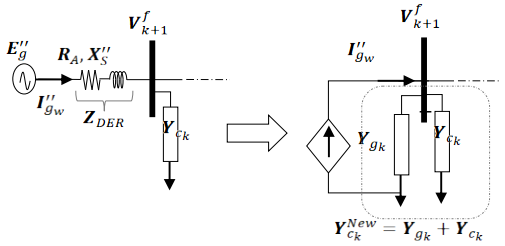

Fig. 1. Electrical model for inverter non-interfaced DER

In Fig. 1, it can be seen that E''_g is the internal voltage of the synchronous generator, X''_S is the sub-transient reactance and R_a is the armature resistance. The analyzed period for the FL study is the sub-transient, this ensures the hypothesis that the concatenated flows in the rotor remain constant, similarly to the internal voltage. This consideration allows determining the internal voltage of the synchronous generator (E''_g) in the pre-fault period and to use it in the fault period to estimate the current contribution I_E from of DER [21], [22]. Thus, the INIDER model allows modeling its current contribution to the fault as a constant current injection, as the admittance matrix Y_g can be added to the system configuration as a load, as is given by (4) and (5).

$$[I_E] = [Y_g][E''_g] \quad (4)$$

$$[Y_g] = [Z_w]^{-1} \quad (5)$$

C. DER effect consideration with measurements provided by IED

When IEDs are installed in the terminals of DER, its effect on the FL can be considered by synchronized phasors measurements. The use of such measurements is presented in the following sections.

III. Generalized FL Equations

FL analysis is reduced to the analyzed line section represented through its exact line segment model, as shown in Fig. 2. Different faults types can be obtained from the combination of switches s1, s2, s3 and s4.

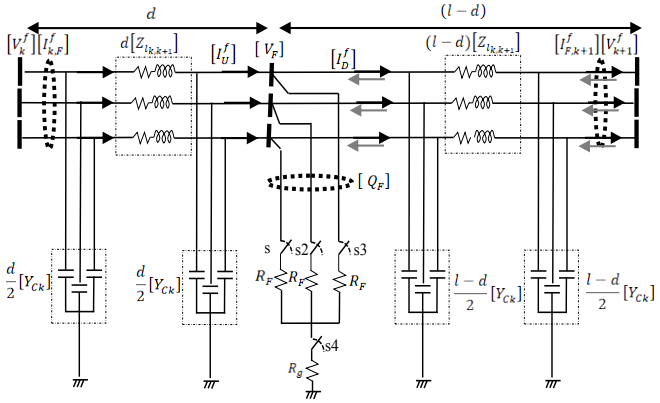

Fig. 2. Modelling of distribution line in fault condition

The behavior of low impedance faults are purely resistive [26]. Taking this into account, we define Q_F as the reactive power consumed by the fault as (6).

$$Q_F = \left[\sum_{w \in \Omega_w} \Im\{V_{F_w} \cdot I^*_{F_w}\}\right] = 0, \quad (6)$$

Where, $\Im\{\cdot\}$ represents the imaginary part of complex numbers, * denotes a complex conjugate, Ω_w is the set of faulted phases, V_{F_w} is the fault point voltage on phase w (Volts) and I_{F_w} is the fault current on phase w (Amps). From Fig. 2, V_{F_w} and I_{F_w} are obtained by (7) and (8), respectively.

$$V_{F_w} = V_{k_w} + d^2 \cdot 0.5 \cdot \Delta v_w - d \cdot \Delta u_w, \quad (7)$$

$$I_{F_w} = I_{U_w} - I_{D_w}, \quad (8)$$

$$\Delta v_w = \sum_{g=\{a,b,c\}} Z_{l_{wg}} \cdot \left(\sum_{h=\{a,b,c\}} Y_{c_{wh}} \cdot V^f_{k_h} \right) \quad (9)$$

$$\Delta u_w = \sum_{g=\{a,b,c\}} Z_{l_{wg}} \cdot I_{kF_g} \quad (10)$$

And d is the fault distance (km), $Z_{l_{wg}}$ is the element wg of the line series impedance matrix (Ohms/km), $Y_{c_{wh}}$ is the element wh of the line shunt admittance matrix (Ohms/km), $V_{k_h}^f$ is the terminal k voltage on phase h (Volts), and I_{kF_g} is the current kF on phase g (Amps). I_{U_w} and I_{D_w} are the currents on phase w that feed the fault as shown in Fig. 2. Replacing (7) into (6), is obtained (11) and (12).

$$Q_F = \left[\sum_{w\in\Omega_w} \Im\left\{\left(V_{k_w} + d^2 \cdot 0.5 \cdot \Delta v_w - d \cdot \Delta u_w\right) \cdot I_{F_w}^*\right\}\right] = 0, \quad (11)$$

$$Q_F = 0.5 \cdot d^2 \cdot \sum_{w\in\Omega_w} \Im\{\Delta v_w \cdot I_{F_w}^*\} - d \cdot \sum_{w\in\Omega_w} \Im\{\Delta u_w \cdot I_{F_w}^*\} + \sum_{w\in\Omega_w} \Im\{V_{k_w} \cdot I_{F_w}^*\} = 0 \quad (12)$$

Equation (12) can be rewrite as a second-order polynomial in x as shown in (13).

$$a_2 \cdot d^2 + a_1 \cdot d + a_0 = 0 \quad (13)$$

where a_0, a_1 and a_2 are given by (14), (15) and (16), respectively.

$$a_0 = \sum_{w\in\Omega_w} \Im\{V_{k_w} \cdot I_{F_w}^*\} \quad (14)$$

$$a_1 = -\sum_{w\in\Omega_w} \Im\left\{\left(\sum_{g=\{a,b,c\}} Z_{l_{wg}} \cdot I_{kF_g}\right) \cdot I_{F_w}^*\right\} \quad (15)$$

$$a_2 = \sum_{w\in\Omega_w} \Im\left\{\left(\sum_{g=\{a,b,c\}} Z_{l_{wg}} \cdot \left(\sum_{h=\{a,b,c\}} Y_{c_{wh}} \cdot V_{k_h}^f\right)\right) \cdot I_{F_w}^*\right\} \quad (16)$$

Two mathematical solutions are possible for (13). The fault distance, d, that represents the physically correct solution, can be identified as presented in [27]. Section 4 presents an algorithm that apply the FL formulation in each line section of the MG, until the fault section is identified.

IV. FL Model and Algorithm

The FL algorithm is divided into four data processing steps, as illustrated in Fig. 3. The steps are explained in the following subsections.

A. Step 1: Processing information of ADN, substation fault records and DER information

In this step, MG system data, such as its topology and the parameters of loads and lines are uploaded. Fault voltage and current phasors recorded in the main substation are estimated [26]. Then, considering initially the DER information available, it is processed. For each DER with available IED in their terminals, measured fault current phasors are considered. In cases when IED are not installed in the terminals of DER, or their information is not available, DER electrical models previously presented are used.

B. Step 2: Estimation of the fault distance in each line section

As the fault line section is unknown, the generalized FL equation (13) is applied to each section of the MG, until faulty line section is identified. This fault line section is identified when a fault distance d estimate is smaller than the length of the line section analyzed ($d^{(s)} < l_k$), as shown in Fig. 2. However, to estimate the fault distance, the fault current has to be estimated first. From Fig. 2, the fault current vector is defined as shown in (17).

$$[\boldsymbol{I}_F] = [\boldsymbol{I}_U^f] - [\boldsymbol{I}_D^f] \quad (17)$$

$$[\boldsymbol{I}_U^f] = -[\boldsymbol{\alpha}_d] \cdot [\boldsymbol{V}_k^f] + [\boldsymbol{\beta}_d] \cdot [\boldsymbol{I}_{k,F}^f] \quad (18)$$

$$[\boldsymbol{\beta}_d] = [\boldsymbol{I}] + 0.5 \cdot d^2 \cdot [\boldsymbol{Z}_{l_{k,k+1}}] \cdot [\boldsymbol{Y}_{C_k}] \quad (19)$$

$$[\boldsymbol{\alpha}_d] = d \cdot [\boldsymbol{Y}_{C_k}] + 0.25 \cdot d^3 \cdot [\boldsymbol{Y}_{C_k}] \cdot [\boldsymbol{Z}_{l_{k,k+1}}] \cdot [\boldsymbol{Y}_{C_k}] \quad (20)$$

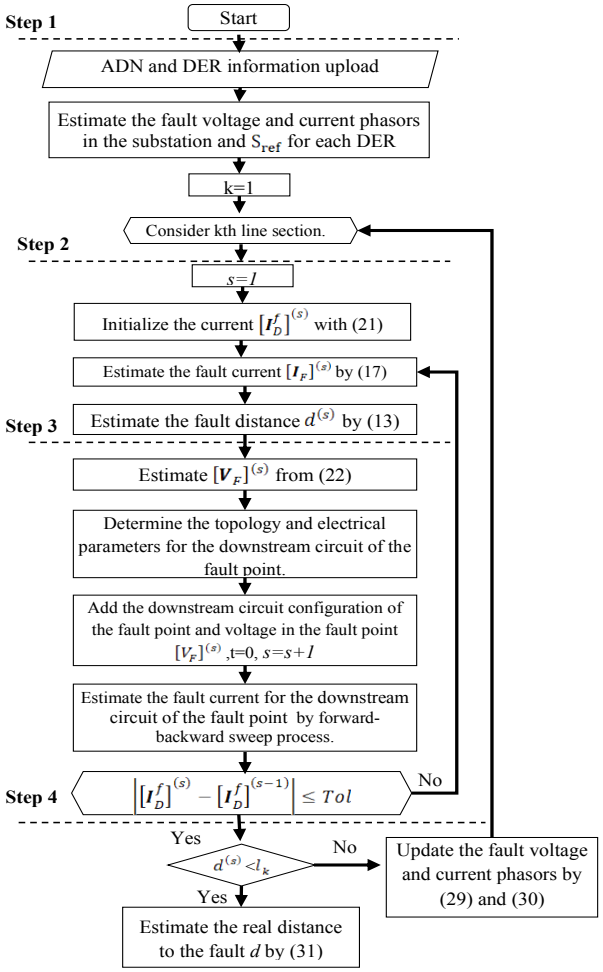

Fig. 3. Flowchart of the FL algorithm

And $[\boldsymbol{I}_D^f]$ is the current downstream to the fault point and is estimated from a forward-backward sweep process as explained in the following, step 3. As the distance d depends on the current $[\boldsymbol{I}_D^f]$ and this current is defined as a function of d, an iterative process to refine the current $[\boldsymbol{I}_D]$ is performed as shown in Fig. 3. Thus, the current $[\boldsymbol{I}_D^f]$ is initialized as the pre-fault (p) current in terminal k, as defined in (21).

$$[\boldsymbol{I}_D^f] = [\boldsymbol{I}_{k,F}^p] \quad (21)$$

C. Step 3: Estimation of the fault current contribution from the downstream circuit to the fault point.

A forward-backward sweep process is used to estimate the current $[\boldsymbol{I}_D^f]$, given that this current depends on the current contribution from DER. This process is applied to the

downstream circuit of the fault point, considering the voltage at the fault point given by (22) as the supply voltage.

$$[\boldsymbol{V}_F] = \left[\boldsymbol{V}_k^f\right] + 0.5 \cdot d^2 \cdot [\Delta \boldsymbol{v}] - d \cdot [\Delta \boldsymbol{u}] \quad (22)$$

$$[\Delta \boldsymbol{v}] = \left[\boldsymbol{Z}_{l_{k,k+1}}\right] \cdot \left[\boldsymbol{Y}_{C_k}\right] \cdot \left[\boldsymbol{V}_k^f\right] \quad (23)$$

$$[\Delta \boldsymbol{u}] = \left[\boldsymbol{Z}_{l_{k,k+1}}\right] \cdot \left[\boldsymbol{I}_{k,F}^f\right] \quad (24)$$

The forward-backward sweep process is composed of two sweeps: a backward sweep and a forward sweep. In the backward sweep, the three-phase voltage vectors are estimated with (25), using the line currents estimated in the previous iteration. In the first iteration, the voltages of the system are initialized as the voltage in the fault point ($[\boldsymbol{V}_k] = [\boldsymbol{V}_F]$).

$$\left[\boldsymbol{V}_{k+1}^f\right] = [\boldsymbol{A}] \cdot \left[\boldsymbol{V}_k^f\right] - [\boldsymbol{B}] \cdot \left[\boldsymbol{I}_{k+1}^f\right] \quad (25)$$

Similarly, forward-sweep estimates the voltage and current phasors in all the nodes. This process is carried out, starting from the farthest nodes to the source node. Fig. 4 illustrates this process.

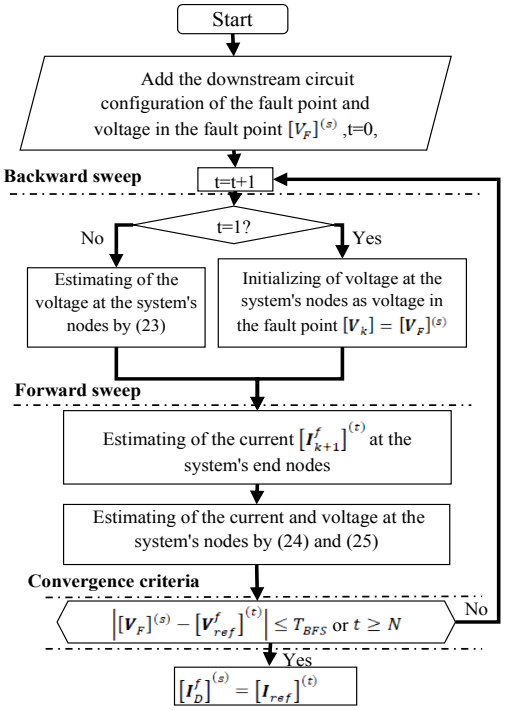

Fig. 4. Fault current estimation flowchart.

The states are estimated through (26) and (27) using the three-phase voltage estimated in the previous iteration.

$$\left[\boldsymbol{V}_k^f\right] = [\boldsymbol{a}] \cdot \left[\boldsymbol{V}_{k+1}^f\right] + [\boldsymbol{b}] \cdot \left[\boldsymbol{I}_{k+1}^f\right] \quad (26)$$

$$\left[\boldsymbol{I}_k^f\right] = [\boldsymbol{c}] \cdot \left[\boldsymbol{V}_{k+1}^f\right] + [\boldsymbol{d}] \cdot \left[\boldsymbol{I}_{k+1}^f\right] \quad (27)$$

where, $[\boldsymbol{A}], [\boldsymbol{B}], [\boldsymbol{a}], [\boldsymbol{b}][\boldsymbol{c}]$ and $[\boldsymbol{d}]$ are the impedance matrices for series feeder components. These impedance matrices are defined in [28].

Thus, when the algorithm initiates, the three-phase current vectors $\left[\boldsymbol{I}_{k+1}^f\right]$ in the end nodes are estimated using the voltage vector computed in the previous iteration and the model of the component connected. Table I presents the components and the expression used in the estimation of $\left[\boldsymbol{I}_{k+1}^f\right]$.

With the currents $\left[\boldsymbol{I}_{k+1}^f\right]$ in the end nodes estimated, equations (26) and (27) are applied to compute the three-phase voltage and current vectors in all the system's nodes.

TABLE I

ESTIMATION OF $\left[I_{k+1}^f\right]$ IN THE END NODES FROM MODELS OF THE COMPONENT CONNECTED.

Component		Description	Equation
shunt components		loads or capacitor banks. Admittance matrices are defined in [28].	$[I_{k+1}^f] = [Y_{k+1}][V_{k+1}^f]$
DER	with IED available	$[\boldsymbol{I}_{k+1}^f]$ is defined from synchronized phasors provided by IED $[\boldsymbol{I}_{IED}^f]$.	$[I_{k+1}^f] = -[I_{IED_{k+1}}^f]$
	without IED available	$[\boldsymbol{I}_S]$ is estimated in function of the inverter operation modes by (1).	$[I_{k+1}^f] = -[I_S]$
		$[\boldsymbol{I}_E]$ is estimated in function of the internal voltage of the synchronous generator and the sub-transient reactance as shown in (4).	$[I_{k+1}^f] = -[I_E]$

Finally, the forward and backward sweeps process are carried out until achieve a convergence criteria given by (28).

$$\left|[\boldsymbol{V}_F] - \left[\boldsymbol{V}_{ref}^f\right]\right| \leq T_{BFS} \quad (28)$$

D. Step 4: Update voltages and current vector and distance from the substation up to the fault point

If the fault is estimated downstream the first system section, then the values of voltage and current measured at the local terminal are updated to the next system buses by (29) and (30).

$$\left[\boldsymbol{V}_{k+1}^f\right] = [\boldsymbol{\beta}_l] \cdot \left[\boldsymbol{V}_k^f\right] - l_{k,k+1} \cdot \left[\boldsymbol{Z}_{\boldsymbol{k,k+1}}\right]\left[\boldsymbol{I}_{k,k+1}^f\right] \quad (29)$$

$$\left[\boldsymbol{I}_{k+1,k+2}^f\right] = -[\boldsymbol{\alpha}_l] \cdot \left[\boldsymbol{V}_k^f\right] + [\boldsymbol{d}_l]\left[\boldsymbol{I}_{k,k+1}^f\right] - \left[\boldsymbol{I}_{L_{k+1}}^f\right] + \left[\boldsymbol{I}_{DER}^f\right] \quad (30)$$

Where $[\boldsymbol{\beta}_l]$, and $[\boldsymbol{\alpha}_l]$ are obtained by (17) and (18) with $d = l_{k,k+1}$, being $l_{k,k+1}$ the current line section length. $\left[\boldsymbol{I}_{DER}^f\right]$ is the current contribution from laterals that have DERs and are connected at node k+1, which is estimated by the ladder-based technique. Besides, after estimating the fault point, the distance d_s from the substation to the fault is also estimated by (31).

$$d_s = \sum_{i=1}^{nt-1} L_i + d \quad (31)$$

V. CASE STUDY

The presented FL algorithm is validated considering the *IEEE* 34-nodes test feeder [29]. This feeder is located in the state of Arizona (USA) and operated at a voltage level of 24.9 kV. Its main features are the presence of single, two-phase, and three-phase laterals, multiple wire sizes as well as unbalanced loads. The system is modeled in ATP–EMTP and modified by adding several DER, which can be IIDER or INIDER, depending on the case evaluated in Table II and as is illustrated in Fig. 5. The INIDER was modelled as a source behind an impedance [21] and IIDER by the fault response of IIDER presented in [25]. IIDER was programmed in ATP-EMTP by using MODELS tool [30]. System loads are modelled as constant impedances. The presented method was validated considering five scenarios. Table II presents a summary of the tests performed to validate the proposed method.

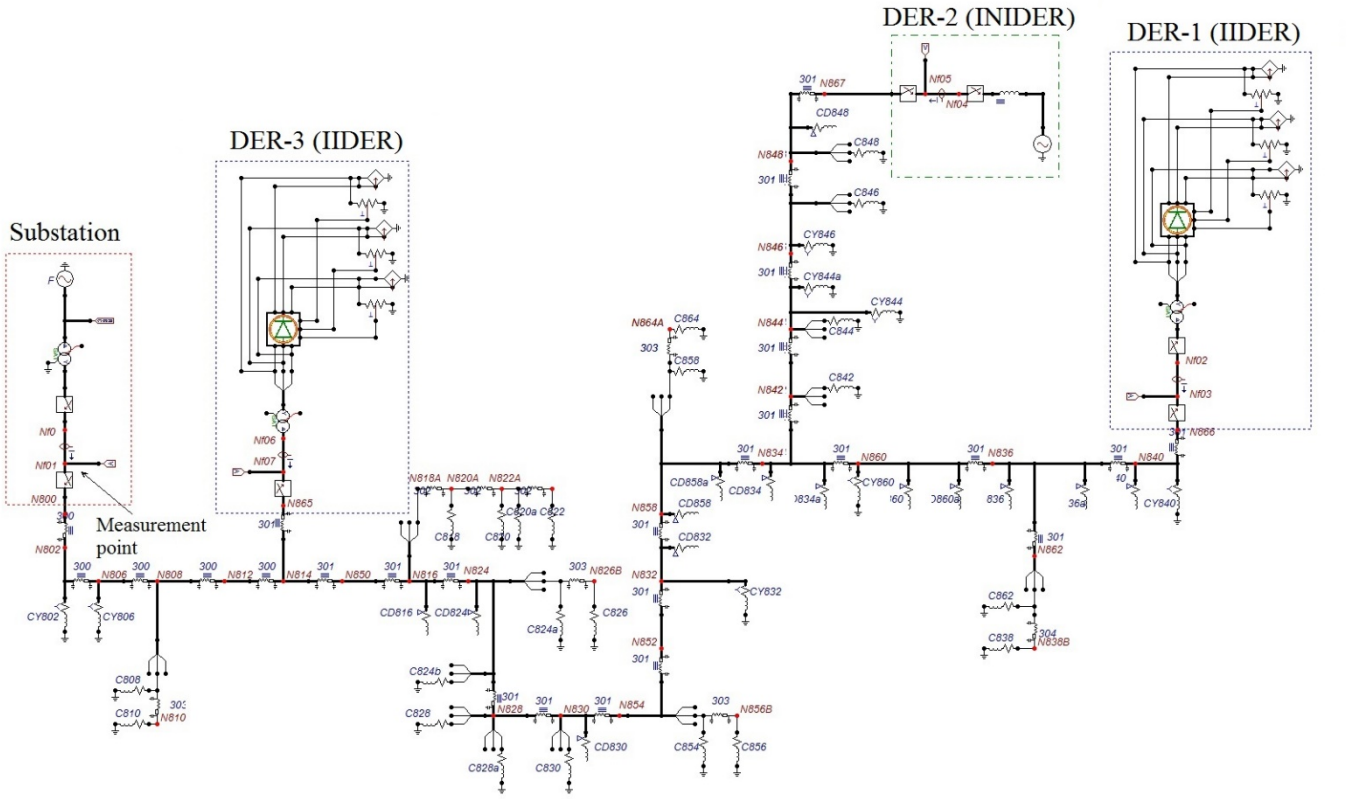

Fig. 5. IEEE 34-node test feeder with integration of DER.

VI. Test Results and Discussion

The results obtained were evaluated considering an error given by (32):

$$error = d_{real} - d_{est} \quad (32)$$

where, $error$ is the relative error given in kilometers, d_{real} is the real fault distance in kilometers, simulated in ATP/EMTP, d_{est} is the estimated fault distance in kilometers. The length of MG is 57.8 km.

The following subsections present the results obtained for the scenarios proposed in Table II.

A. Scenario 1: Effect of fault resistance

For this scenario, the DER effect is considered as follows:

DER1-linear analytical equivalent models for the different inverter operation modes; DER2-the approximate model of the synchronous generator and DER3-synchronized current phasors provided by IED. All simulated faults are located in the primary feeder. Test results are presented by performance curves, as shown in Fig. 6. Further, statistics of the estimation error are also presented, through a boxplot, as shown in Fig. 6.

The boxplot shows the distribution of errors for each fault type and for each fault resistance range for the proposed method. From Fig. 6 one can observe an increase of the error when the fault resistance increases. Thus is an expected effect on impedance-based FL methods, since as the fault resistance increases, it tends to be comparable with the system impedance observed from the substation and this feature affects the FL methods performance [31]. Nonetheless, the errors obtained for this scenario show the efficiency and robustness of the proposed method, with maximum errors of less than 800 m for fault resistance of 100Ω in a 57.8 km feeder.

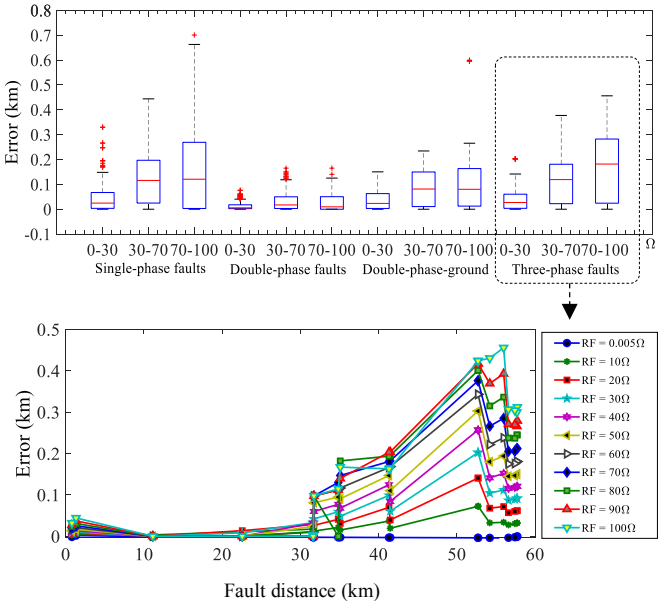

Fig. 6. Effect of fault resistance on the proposed method.

TABLE II
FAULT SCENARIOS TO VALIDATE THE PROPOSED FL APPROACH

Scenario	Description	Faults
Effect of the fault resistance	Fault location: all nodes of the primary feeder	2299
	Fault type: all	
	Fault resistance between: 0.0005Ω-100Ω	
	Number of the DER connected: 3	
	DER penetration level: 10% for each unit	
Effect of DER penetration level	Fault type: single-phase faults	171
	Fault resistance: 10Ω	
	DER penetration level: 10%, 20%, 30%	
	Number of the DER connected: 1	
	DER type: IIDER and INIDER	
Effect of errors of DER information	DER penetration level: 30%	171
	Number of the DER connected: 1	
	Error in the current phasors: ±10%, ±30%	
	DER type: INIDER	
	Error in the sub-transient reactance: ±10%, ±30%	
	DER type: INIDER	
	Error in the power set-point: ±10%, ±30%	
	DER type: IIDER	
Effect of number of DER connected	case 1: Number of DER connected: 1 , bus 840	171
	DER penetration level: 30%	
	case 2: Number of DER connected: 2, bus 840, 848	
	DER penetration level: 15% for each unit	
	case 3: Number of DER connected: 3, bus 840, 848 and 814	
	DER penetration level: 10% for each unit	
	DER type: IIDER and INIDER	
Effect of random load variation	Random load variation: 30-60%, 60-100% and 100-150%	51
	Fault type: single-phase faults	
	Number of the DER connected: 3	
	DER penetration level: 10% for each unit	
Total		2863

B. Scenario 2: Effect of DER penetration level

For this scenario, two cases are analyzed: effect of INIDER penetration level and effect of IIDER penetration level. For the first case, the synchronized current phasors provided by IED and the approximate model of the synchronous generator are used to consider the DER effect. In the second case, linear analytical equivalent models for the different inverter operation modes are used to consider the DER effect. The results are presented in a performance curve, which shows the percentage error as a function of the fault distance.

Fig. 7 to 9 present the performance for the proposed method under DER penetration level effect. The results show an effect to estimate a distance smaller than the real fault distance, as the DER penetration level increases. This behavior occurs because the error associated with the estimation of the current contribution increases with the DER penetration level. Thus, this error induces estimating a current contribution greater than the real current contribution. Therefore, a greater fault current is estimated, which makes the proposed method estimates a smaller fault distance. However, for both considerations, i.e. when the synchronized current phasors provided by IED or the linear analytical equivalent models of the DER are used; the method performance is satisfactory, presenting estimation errors smaller than 600 m.

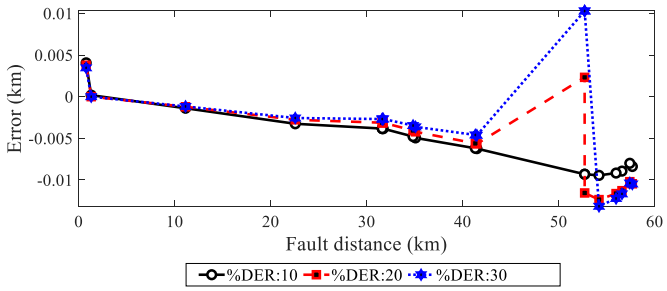

Fig.7. Effect of DER penetration level on the proposed method using the synchronized current phasors provide by IED

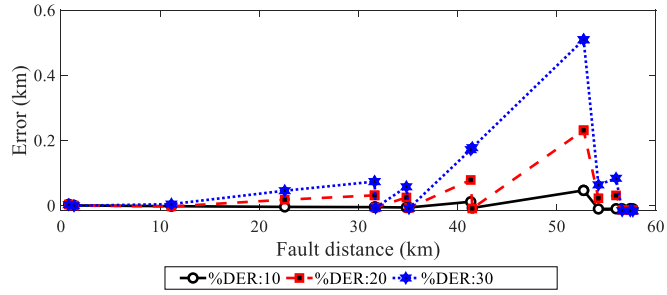

Fig.8. Effect of DER penetration level on the proposed method using the approximate model of the synchronous generator.

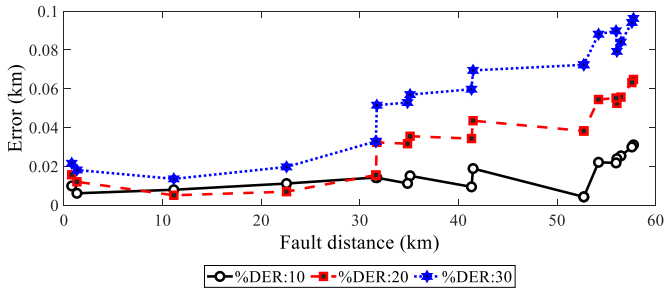

Fig.9. Effect of DER penetration level on the proposed method using the linear analytical equivalent models for the different inverter operation modes.

C. Scenario 3: errors on DER information

The results for this scenario are presented in Fig.10, 11 and 12.

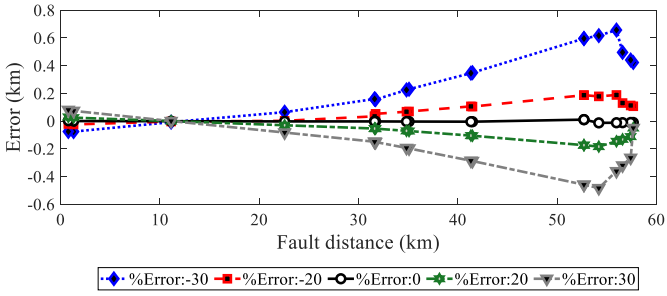

Fig.10. Effect of errors of DER information on the proposed method using the synchronized current phasors provided by IED

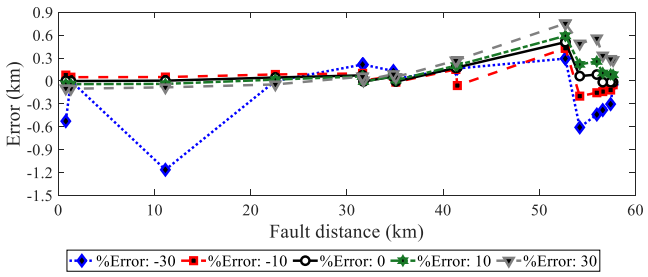

Fig.11. Effect of error of DER information (sub-transient reactance) on the proposed method using the approximate model of the synchronous generator.

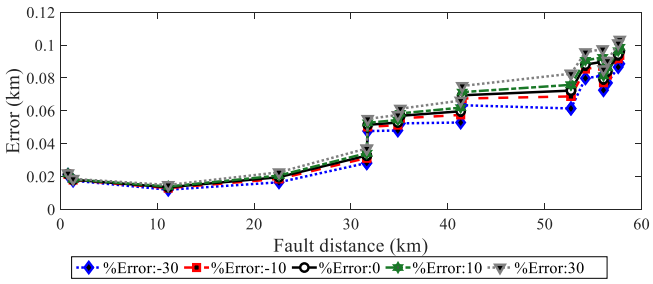

Fig.12. Effect of errors of DER information (power set-point S_{ref}) on the proposed method using the linear analytical equivalent models for the different inverter operation modes.

Fig. 10 presents the performance for the proposed method considering errors the current phasors provided by IED. The results indicate that the proposed method presents sensitivity to errors on the measurements. One can observe that for errors between ± 30% on the DER's current phasor, there are maximum errors of ±800 m in the fault distance estimation. In the same way, test results show a correlation between the method's performance and the characteristic of the errors. Thus, for negative errors, errors that infer a lower current phasor estimation, the method's effect is to estimate a fault distance smaller than the real distance to the fault point, and vice-versa.

Similarly, Fig. 11 presents the presented methods performance under error in the sub-transient reactance. For this scenario, a small sensitivity for sub-transient reactance errors is observed. However, when the error is increased significantly, the method increases its computational time, evidencing difficulty for its convergence and in one case finishing the ladder-based technique by number of iterations. This case is reflects in an high estimation error. On the other hand, Fig. 12 shows the proposed method performance under errors in the power set-point S_{ref}. Similarly, to the first case, there is a correlation between the method's performance and the errors in S_{ref} estimation. This weak correlation shows a low sensitivity of the proposed method to the errors in the estimation of S_{ref}, where one case observe estimation errors smaller than 120 m.

D. Scenario 4: Effect of number of DER connected

To analyze the effect of the number of DER connected, three cases showed in the Table II were studied. The results for this scenario are presented in Fig. 13, 14 and 15. Test results show a similar behavior for the method's performance when 1 or 2 DER are connected into MG. Nevertheless, an increase in the estimation error appears when a third DER unit is connected. This error is associated with the location of DER-3. This shows that the presented method is sensitive to DER allocation. However, this sensitivity does not significantly affect the method's performance. The maximum errors obtained for this scenario are 15 m, 180 m, and 600 m in a 57.8 km feeder for the Fig.13 to 15 respectively.

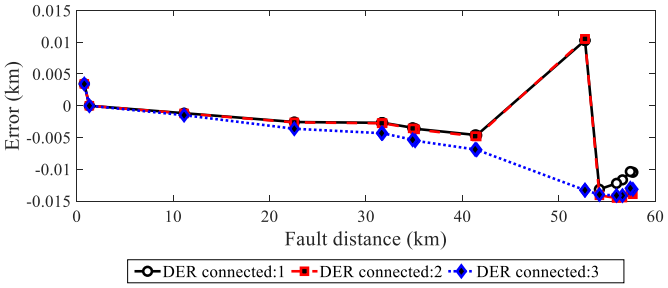

Fig.13. Effect of number of DER connected on the proposed method using the synchronized current phasors provide by IED

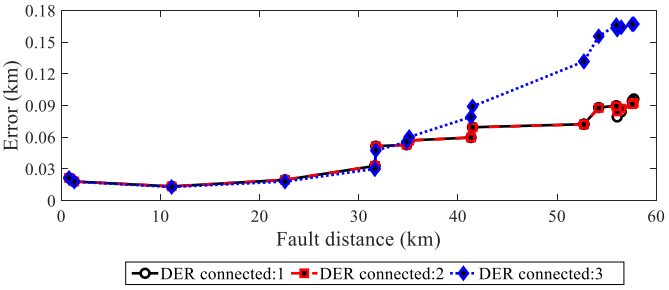

Fig.14 Effect of number of DER connected on the proposed method using the linear analytical equivalent models for the different inverter operation modes.

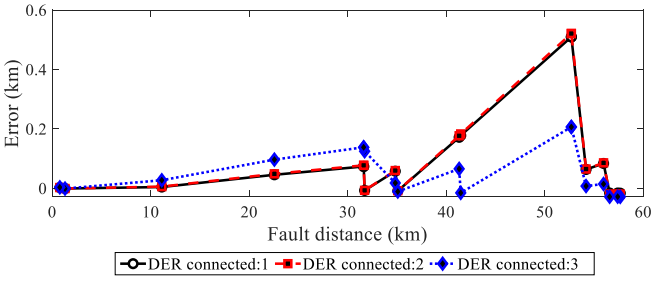

Fig.15. Effect of number of DER connected on the proposed method using the approximate model of the synchronous generator.

E. Scenario 5: Effect of random load variation

The results for this scenario are presented in the Fig. 16.

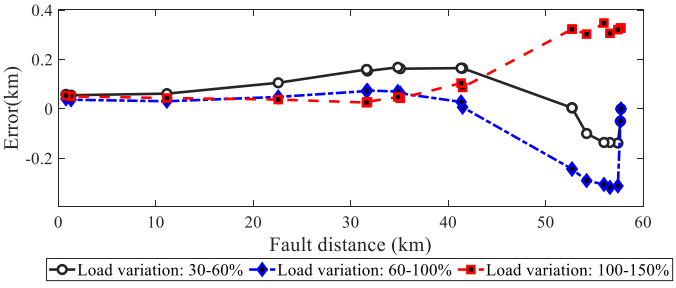

Fig.16. Effect of random load variation.

For test results obtained with a random load variation of 100% -150%, the presented method exposed an underestimation behavior of the fault distance. However, for scenarios where a lower load on the system was considered (random load variation of 30-60% and 60-100%), its behavior

is of underestimation the fault distance in the first line sections and overestimation for the last line sections of the network. This behavior appears since the load variation is not compensated, making the method, for the first sections, to consider a higher load since it uses the nominal load of the system. Thus, a lower impedance is observed by the approach and, therefore, a smaller distance to the fault. For the last line sections, the methodology observes a higher impedance due to when updating currents at the local terminal, a greater load is considered. Consequently, this causes a lower current in the next section to be estimated and, therefore, the proposed method estimates a higher distance to the fault. The previous shows that, the proposed method presents a small sensitivity to load variations.

VII. Conclusion

This paper presents analytical physics-based models towards FL in MG. The presented method uses a backward-forward sweep process to consider the effect of different DER technologies in the fault location formulation. Wide-area synchronized measurements are considered, when available. Small estimation errors in the fault distance are obtained for all fault scenarios evaluated. That said, when considering wide-area measurements, high sensitivity to measurement errors are highlighted. Presented models are flexible considering the effect of the DER, through synchronized current measurements provided by IEDs or using local information through the linear analytical equivalent models of DER. This guarantees that, if there is a lack of communication or synchronism between the measurements, the fault location can be still estimated. Test results demonstrated the accuracy and robustness of the presented method under several effects such as: fault resistance, DER penetration level, numbers of DERs connected, load variation and errors in the DER information.

VIII. References

[1] M. J. Ghadi, A. Rajabi, S. Ghavidel, A. Azizivahed, L. Li, and J. Zhang, "From active distribution systems to decentralized microgrids: A review on regulations and planning approaches based on operational factors," *Appl. Energy*, vol. 253, no. March, 2019.

[2] N. Hatziargyriou, *Microgrids: Architectures and Control*. John Wiley & Sons Ltd, 2014.

[3] A. Bahmanyar, S. Jamali, A. Estebsari, and E. Bompard, "A comparison framework for distribution system outage and fault location methods," *Electr. Power Syst. Res.*, vol. 145, pp. 19–34, 2017.

[4] P. Kumar, V. Kumar, and R. Pratap, "Design and verification of hardcore reconfigurable relay for islanding detection and subsequent mode adaptation of microgrid," *Int. Trans. Electr. Energy Syst.*, no. November 2018, pp. 1–19, 2019.

[5] M. Shafiullah, M. A. Abido, and T. Abdel-Fattah, "Distribution grids fault location employing ST based optimized machine learning approach," *Energies*, vol. 11, no. 9, 2018.

[6] E. Correa-Tapasco, J. Mora-Flórez, and S. Perez-Londoño, "Performance analysis of a learning structured fault locator for distribution systems in the case of polluted inputs," *Electr. Power Syst. Res.*, vol. 166, no. August 2018, pp. 1–8, 2019.

[7] E. Correa-Tapasco, J. Mora-Flórez, and S. Pérez-Londoño, "Robustness of a generalized impedance based fault locator considering distorted measurements," *Electr. Power Syst. Res.*, vol. 154, pp. 234–244, 2018.

[8] M. A. Gabr, D. K. Ibrahim, E. S. Ahmed, and M. I. Gilany, "A new impedance-based fault location scheme for overhead unbalanced radial distribution networks," *Electr. Power Syst. Res.*, vol. 142, pp. 153–162, 2017.

[9] H. Cifuentes-Chaves, J. Mora-Flórez, and S. Pérez-Londoño, "Time domain analysis for fault location in power distribution systems considering the load dynamics," *Electr. Power Syst. Res.*, vol. 146, pp. 331–340, 2017.

[10] M. T. Rahman Dashti, Seyed Mehdi Salehizadeh, Hamid Reza Shaker, "Fault Location in Double Circuit Medium Power Distribution Networks Using an Impedance-Based Method," *Appl. Sci.*, pp. 1–15, 2018.

[11] S. Jamali, A. Bahmanyar, and E. Bompard, "Fault location method for distribution networks using smart meters," *Measurement*, vol. 102, pp. 150–157, 2017.

[12] S. Jamali and A. Bahmanyar, "A new fault location method for distribution networks using sparse measurements," *Int. J. Electr. Power Energy Syst.*, vol. 81, pp. 459–468, 2016.

[13] M. J. S. Ramos, A. S. Bretas, D. P. Bernardon, and L. L. Pfitscher, "Distribution networks HIF location : A frequency domain system model and WLS parameter estimation approach," *Electr. Power Syst. Res.*, vol. 146, pp. 170–176, 2017.

[14] J. U. N. Nunes, A. S. Bretas, N. G. Bretas, A. R. Herrera-Orozco, and L. U. Iurinic, "Distribution systems high impedance fault location: A spectral domain model considering parametric error processing," *Int. J. Electr. Power Energy Syst.*, vol. 109, no. January, pp. 227–241, 2019.

[15] R. Perez, C. Vásquez, and A. Viloria, "An intelligent strategy for faults location in distribution networks with distributed generation," *J. Intell. Fuzzy Syst.*, vol. 36, no. 2, pp. 1627–1637, 2019.

[16] C. Orozco-Henao, A. Bretas, R. Leborgne, A. Herrera, and S. Martinez, "Fault Location in Distribution Network with Inverter- Interfaced Distributed Energy Resources in Limiting Current," in *2016 17th International Conference on Harmonics and Quality of Power (ICHQP)*, 2016, pp. 231–236.

[17] C. Orozco-Henao, A. S. Bretas, A. R. Herrera-Orozco, J. D. Pulgarín-Rivera, S. Dhulipala, and S. Wang, "Towards active distribution networks fault location: Contributions considering DER analytical models and local measurements," *Int. J. Electr. Power Energy Syst.*, vol. 99, no. September 2017, pp. 454–464, 2018.

[18] K. Jia, C. Gu, L. Li, Z. Xuan, T. Bi, and D. Thomas, "Sparse voltage amplitude measurement based fault location in large-scale photovoltaic power plants," *Appl. Energy*, vol. 211, no. June 2017, pp. 568–581, 2018.

[19] C. Orozco-Henao, A. Suman Bretas, J. Marín-Quintero, A. Herrera-Orozco, J. Pulgarín-Rivera, and J. Velez, "Adaptive Impedance-Based Fault Location Algorithm for Active Distribution Networks," *Appl. Sci.*, vol. 8, no. 9, p. 1563, 2018.

[20] F. M. Aboshady, M. Sumner, and D. W. P. Thomas, "A Wideband Fault Location Scheme for Active Distribution Systems," in *2018 7th International Conference on Renewable Energy Research and Applications (ICRERA)*, 2018, vol. 5, pp. 891–896.

[21] J. U. N. Nunes and A. S. Bretas, "An Extended Fault Location Formulation for Unbalanced Distribution Feeders with Distributed Generation," in *International Conference on Power System Technology*, 2011, no. 1, pp. 1–6.

[22] S. Jamali and V. Talavat, "Accurate Fault Location Method in Distribution Networks Containing Distributed Generations," *Iran. J. Electr. Comput. Eng.*, vol. 10, no. 1, pp. 27–33, 2011.

[23] C. Orozco-Henao, A. S. Bretas, R. Chouhy-Leborgne, A. R. Herrera-Orozco, and J. Marín-Quintero, "Active distribution network fault location methodology: A minimum fault reactance and Fibonacci search approach," *Int. J. Electr. Power Energy Syst.*, vol. 84, 2017.

[24] A. Bahmanyar and S. Jamali, "Fault location in active distribution networks using non-synchronized measurements," *Int. J. Electr. Power Energy Syst.*, vol. 93, pp. 451–458, 2017.

[25] C. A. Plet and T. C. Green, "Fault response of inverter interfaced distributed generators in grid-connected applications," *Electr. Power Syst. Res.*, vol. 106, pp. 21–28, Jan. 2014.

[26] M. M. Saha, J. Izykowski, and E. Rosolowski, *Fault Location on Power Networks*. London: Springer, 2010.

[27] R. H. Salim, K. C. O. Salim, and A. S. Bretas, "Further improvements on impedance-based fault location for power distribution systems," *IET Gener. Transm. Distrib.*, vol. 5, no. 4, p. 467, 2011.

[28] W. Kersting, *Distribution System Distribution Syste Modeling and Analysis*. New Mexico Boca: CRC Press, 2012.

[29] Distribution System Analysis Subcommittee, "IEEE 34 Node Test Feeder." 2001.

[30] L. Dubé, "Users Guide To MODELS in ATP," 1996.

[31] D. Gazzana, G. Ferreira, A. S. Bretas, A. Bettiol, A. Carniato, L.F. Passos, A. H. Ferreira, J. E. M. Silva, "An Integrated Technique for Fault Location and Section Identification in Distribution Systems," *Electr. Power Syst. Res.*, vol. 115, pp. 65–73, Oct. 2014.